OPEN

Phase-controlled synthesis of α-NiS nanoparticles confined in carbon nanorods for High Performance Supercapacitors

Chencheng Sun[1], Mingze Ma[1], Jun Yang[1], Yufei Zhang[1], Peng Chen[3], Wei Huang[1,2] & Xiaochen Dong[1,2]

[1]Key Laboratory of Flexible Electronics (KLOFE) & Institute of Advanced Materials (IAM), Jiangsu National Synergistic Innovation Center for Advanced Materials (SICAM), Nanjing Tech University (Nanjing Tech), 30 South Puzhu Road, Nanjing 211816, P. R. China, [2]Key Laboratory for Organic Electronics & Information Displays (KLOEID), Nanjing University of Posts and Telecommunications, Nanjing China, 210023, [3]School of Chemical and Biomedical Engineering, Nanyang Technological University 62 Nanyang Drive, Singapore, 637459.

Correspondence and requests for materials should be addressed to P.C. (chenpeng@ntu. edu.sg); W.H. (iamwhuang@njtech. edu.cn) or X.C.D. (iamxcdong@njtech. edu.cn)

A facile and phase-controlled synthesis of α-NiS nanoparticles (NPs) embedded in carbon nanorods (CRs) is reported by in-situ sulfurating the preformed Ni/CRs. The nanopore confinement by the carbon matrix is essential for the formation of α-NiS and preventing its transition to β-phase, which is in strong contrast to large aggregated β-NiS particles grown freely without the confinement of CRs. When used as electrochemical electrode, the hybrid electrochemical charge storage of the ultrasmall α-NiS nanoparticels dispersed in CRs is benefit for the high capacitor (1092, 946, 835, 740 F g^{-1} at current densities of 1, 2, 5, 10 A g^{-1}, respectively.). While the high electrochemical stability (approximately 100% retention of specific capacitance after 2000 charge/discharge cycles) is attributed to the supercapacitor-battery electrode, which makes synergistic effect of capacitor (CRs) and battery (NiS NPs) components rather than a merely additive composite. This work not only suggests a general approach for phase-controlled synthesis of nickel sulfide but also opens the door to the rational design and fabrication of novel nickel-based/carbon hybrid supercapacitor-battery electrode materials.

Nickel sulfide, a transition metal chalcogenide, has recently attracted much attention due to its exceptional electrochemical properties, good electrical conductivity and low cost[1–3]. Interestingly, nickel sulfide can assume various thermodynamically stable crystal structures and stoichiometric forms including NiS, NiS_2, Ni_3S_2, Ni_3S_4, Ni_4S_3, Ni_7S_6 and Ni_9S_8[4–6]. NiS with the simplest stoichiometry exists in two possible phases: α-NiS (hexagonal, $P63/mmc$) and β-NiS (rhombohedral, $R3m$). The former is metalic while the latter is insulating. α-β phase transition can take place under certain conditions, accompanied by 4% volume change[7,8].

The intrinsic properties of a nanomaterial are largely determined by its unique crystal structure[9–11]. As known, the crystal phase of nanocrystals is sensitive to the synthetic conditions including temperature, pressure and reactant composition[12–14]. Therefore, it is important to develop phase-controlled synthesis methods to obtain desired materials for specific applications. It has been shown that crystal structures may be dictated by size constraint *via* crystallization of materials in nanoporous media[15–18]. For instance, Hu et al. have obtained rhombohedral single-crystal nickel sulfide nanowires by confined synthesis in the gaps of silicon dioxide nanospheres[19].

Taking advantages of their high electrochemical activities, both α-NiS and β-NiS have been utilized as the electrode materials[20,21]. α-NiS outperforms β-NiS due to its better conductivity and the fact β-NiS irreversibly transforms to $Ni(OH)_2$ in alkaline solution[22,23]. Current nickel sulfide based supercapacitors and Li-ion batteries, however, are suffered from poor cycling stability due to the agglomeration and pulverization of nickel sulfide materials during repetitive charge/discharge processes[24,25].

In view of these problems, we herein report a facile and phase-controlled synthesis of α-NiS nanoparticles (NPs) embedded in carbon nanorods (denoted as α-NiS/CRs) by in-situ sulfurating the preformed Ni/CRs. The electrode based on such hybrid nanocomposite material demonstrates high specific capacitance (1092 F g^{-1} at 1 A g^{-1} and 740 F g^{-1} at 10 A g^{-1}) and outstanding cycling stability (no apparent capacitance decrease after 2000 cycles).

Results

Precursor characterizations. The Ni/CRs composite was prepared by carbonization of nickel dimethyglyoximate in argon at 350°C for 1 h. As shown in Fig. S1a (Supporting Information), numerous rectangular nanorods (500 nm - 1 μm long and ~100 nm wide) were obtained. The atomic ratio of Ni and C is 18.3 : 81.7 as revealed by energy dispersive spectroscopy (EDS) (Fig. S1b). The spectrum of X-ray diffraction (XRD) displays three prominent peaks which can be perfectly indexed to Ni (JCPDS card No.04-0850) and a weak and broad peak (at ~24°) originated from amorphous carbon (Fig. S1c)[26]. The Ni content was further evaluated by thermogravimetric analysis (TGA) in air. A net weight loss of 36.4% is observed due to oxidation of CRs (≥372°C, causing weight loss) and oxidation of Ni to NiO (≥393°C, causing weight gain) (Fig. S1d)[27]. The Ni content is calculated to be ~50.1 wt. %, which is in accordance with the EDS analysis. This high loading of Ni is superior to other reported Ni/Carbon composites[28–30].

Microstructure characterizations. As illustrated in Fig. 1, α-NiS/CRs composites were exclusively synthesized when Ni/CRs were directly in-situ sulfurated by refluxing in glycerol for 1 h. In comparison, sulfuration of the mixture of Ni NPs and mesoporous CRs (MCRs) leads to formation of β-NiS/CRs composite. MCRs were produced by removing Ni NPs from Ni/CRs via overnight incubation with 3 M HCl. The microstructure of α-NiS/CRs composite was characterized by SEM and TEM which was show in Fig. 2a–2d As revealed by field-emission scanning electron microscopy (FESEM), CRs are decorated with numerous α-NiS NPs after in-situ sulfidation (Fig. 2a). EDS microanalysis indicates that the atomic ratio of Ni/S (12.8/13.1) is closed to the stoichiometry of NiS (Fig. S2). The unaltered C/Ni ratio before and after sulfidation suggests an in-situ nucleation process. Transmission electron microscopy (TEM) shows that α-NiS NPs (black dots) with uniform particle size (~5 nm) are homogenously and densely embedded in the CRs (gray matrix) (Fig. 2b). As reported by previous literatures, the CRs coating can not only partially act as a conductive binder to increase the contact between nanoparticles but also alleviate the aggregation of the active materials and lead to the excellent electrochemical cycling stability[31,32]. High-resolution transmission electron microscopy (HRTEM) in Fig. 2c shows that the d-spacing of the NPs is 0.198 nm, which is in agreement with the d_{102}-spacing of α-NiS (highlighted by dash circles). Uniform dispersion of NiS NPs in the carbon matrix is further confirmed by EDS mapping (Fig. 2d).

In contrast, sulfurating the mixture of Ni NPs and Ni-free MCRs leads to formation of randomly dispersed β-NiS aggregates as shown in SEM and TEM images (Fig. S3a and S3b). The HRTEM image in Fig. S3c reveals the lattice interplanar spacing of ~0.294 nm corresponding to the (101) plane distance of rhombohedral β-NiS. Evidently, the nanopore-confinement is critical to the formation of α-NiS and prevent its possible transformation to β-NiS, since there is a 4% volume expand from α to β phase. So it is believed that the size effect caused by the carbon nanorods may be benefit for the formation of α-NiS.

The identity of two different crystal forms of nickel sulfide obtained from disparate synthetic routes can be confirmed by XRD analysis (Fig. 2e). The two patterns can be unambiguously assigned to α-NiS (hexagonal, *P63/mmc,* JCPDS card No.02-1280) and β-NiS (rhombohedral, *R3m,* JCPDS card No.86-2281), separately. A broad peak located at 26° was attributed the amorphous carbon. Nitrogen physisorption measurements was adopted to further confirm that α-NiS NPs were confined into the CRs. Fig. 2e and 2f show the N_2 adsorption-desorption isotherms of MCRs and α-NiS/CRs (inset are corresponding pore size distribution). The former are nanoporous (narrowly distributed around 5 nm) due to removal of originally embedded Ni NPs whereas the later are no longer nanoporous (the indicated pore size of ~60 nm is from the interstitial space between α-NiS/CRs). Besides, the BET surface area decreased from 200.1 m^2 g^{-1} to 30.8 m^2 g^{-1} after loaded with α-NiS NPs.

Electrochemical properties. We speculate that α-NiS/CRs composite could be a good electrode material for charge storage owing to its unique hierarchical structure, conductive nature and high electrochemical performance expected from α-NiS NPs. Fig. 3a shows the cyclic voltammetry (CV) analysis of bare CRs and the two composites in the potential range of 0–0.50 V (vs. standard calomel electrode). α-NiS/CRs shows a much larger CV area than that from β-NiS/CRs and bare CRs, indicating a higher capacitance (also see CV profiles at different scan rates shown in Fig. S4a and S4c). The redox peaks of α-NiS/CRs is originated from the following NiMH battery-like reaction:

$$NiS + OH^- \rightleftharpoons NiSOH + e^- \quad (1)$$
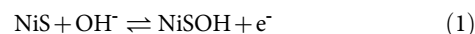
while the redox peaks of β-NiS/CRs (which disappear after the first cycle) is due to the following irreversible reaction[21]:

$$NiS + H_2O + {}^1\!/_2\,O_2 \rightarrow Ni(OH)_2 + S \quad (2)$$

$$Ni(OH)_2 + OH^- \rightleftharpoons NiOOH + H_2O + e^- \quad (3)$$
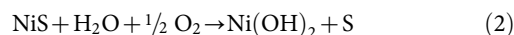
The excellent electrochemical reversibility and kinetics of α-NiS/CRs are evidenced by its symmetric galvanostatic charge/discharge curves, and its higher capacity than that of β-NiS/CRs is indicated by
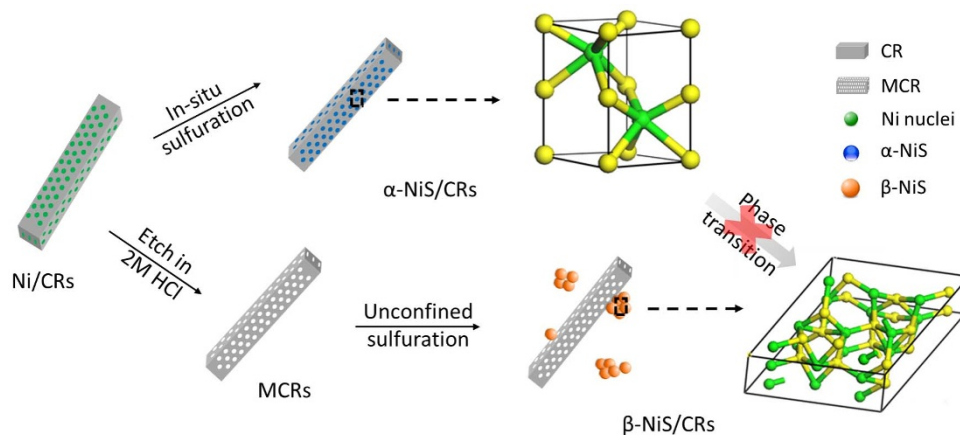

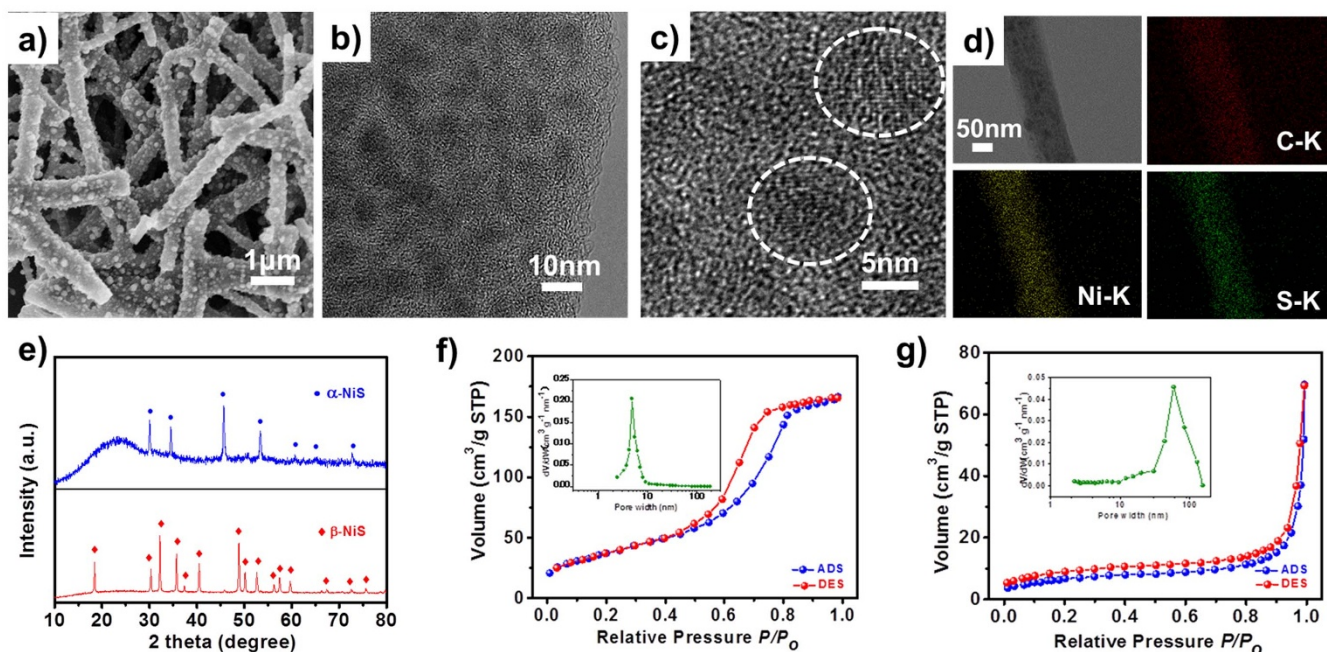**Figure 1 | Schematic illustration for the synthesis of α and β-NiS/CRs composites.**

Figure 2 | **Characterizations of α- and β-NiS/CRs composites.** (a) FESEM, (b) TEM, (c) HRTEM, (d) EDX mapping of α-NiS/CRs; (e) XRD patterns of α- and β-NiS/CRs, and N_2 adsorption-desorption isotherms and corresponding pore size distributions (inset) of mesoporous carbon (f) and α-NiS/CRs composite (g) calculated from BJH model.

its longer charge/discharge time (Fig. S4b and S4d). The specific capacitances calculated based on the galvanostatic charge/discharge curves at different current densities are plotted in Fig. 3b. The α-NiS/CRs electrode exhibits high capacitance of 1092 F g^{-1} at 1 A g^{-1}.

~67.8% of the capacitance retains at the high current density of 10 A g^{-1}. This electrode outperforms the β-NiS/CRs electrode (514 F g^{-1} at 1 A g^{-1}) and the previously reported nickel sulfide based electrodes, such as NiS hollow spheres[33], flower-like β-NiS[21] and
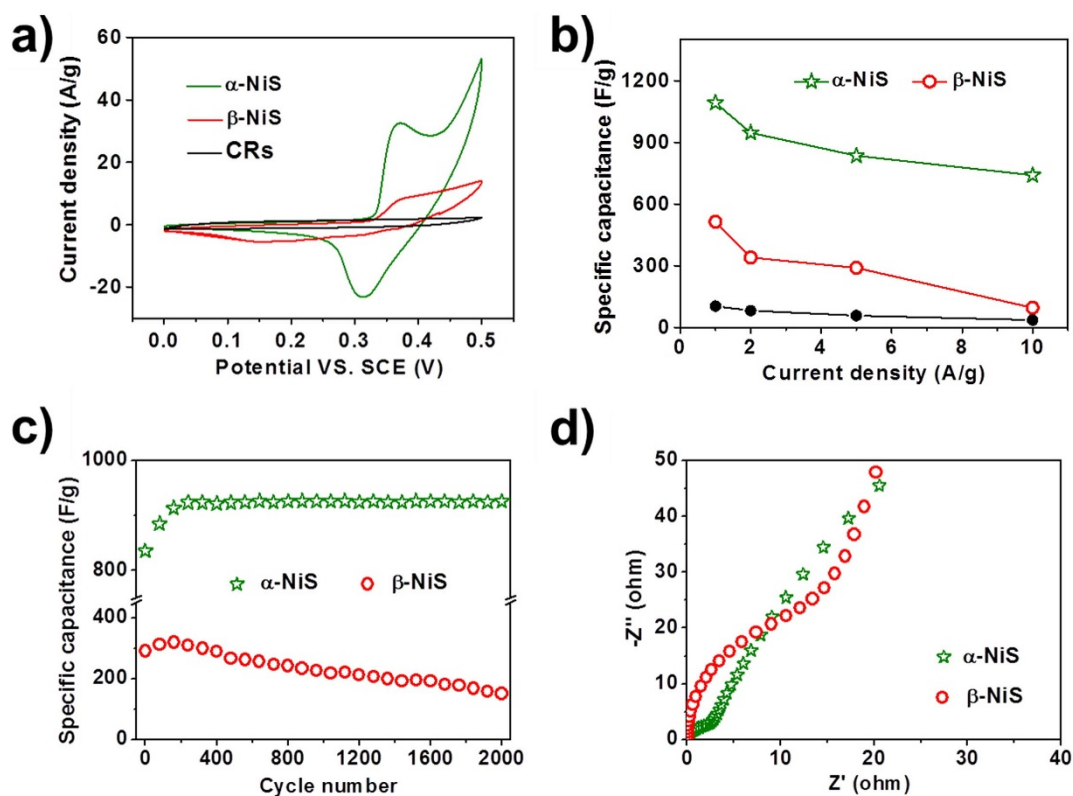

Figure 3 | **Electrochemical properties of α-NiS/CRs, β-NiS/CRs composites and bare CRs.** (a) CV curves of α-, β-NiS/CRs composites and bare CRs at 5 mV s^{-1}. (b) Specific capacitance of α-, β-NiS/CRs composites and bare CRs at various current density. (c) Cycling performance, and (d) Nyquist plots of the EIS of α and β-NiS/CRs composites.

Ni_3S_2-graphene hybrid[25]. The α-NiS NPs well-dispersed into the CRs provide numerous electroactive sites in favor of the high specific capacitance[34].

To evaluate the contribution of each of the components, CV and galvanostatic charge/discharge curves of bare mesopore CRs at various current densities were characterized, as shown in Figure S5. As expected, the bare carbon nanorods showed a typical double layer capacitor behavior with a weak current response and short discharge time compared with α-NiS/CRs composites. After combined with NiS NPs, this "supercapacitor-battery electrode" materials emerged as a hybrid behavior from supercapacitor (at high scan rate) to battery (at low scan rate). As reported by previous literatures[35,36], this kind of hybrid electrode makes a synergistic use of capacitor and battery components rather than a merely additive composite, which gives a significant improvements for the rate performance, cycle lifetime and safety of electrodechemical charge storage devices.

Fig. 3c shows the specific capacitances versus the number of charge/discharge cycles for the two composites at a current density of 5 A g^{-1}. As seen, the specific capacitance of α-NiS/CRs increases from 835 F g^{-1} to 925 F g^{-1} at the first 200 cycles due to activation of the electrode[37]. Afterwards, the capacitance sustains without apparent decrease till 2000 cycles. In contrast, the capacitance of β-NiS/CRs electrode fades away quickly (from 290 F g^{-1} to 144 F g^{-1}, 50.3% loss after 2000 cycles). The high cycling stability is because α-NiS NPs are stably confined and protected within CRs without the issues of aggregation and volume expansion. Fig. 3d presents the electrochemical impedance spectra (EIS) of the two different NiS/CRs composites. The α-NiS/CRs electrode exhibits smaller charge transfer resistance (2.5 Ω indicated as the radius of the preceding semicircle of the Nyquist plot)[38]. This attributable to the high conductivity of carbon nanorodes and readily access of the electrolytes to the electrochemically active sites. Comparison between our α-NiS/CRs electrode and other nickle sulfide electrodes is provided in Table S1.

To demonstrate the electrochemical evolution of the α-NiS/CRs hybrid electrode, EIS and CV measurements were performed before and after 2000 charge/discharge cycles, as shown in Fig. 4a and Fig. 4b. Both EIS and CV characteristics are almost unaltered (the slightly stronger response of final CV curve in accordance with the ~10% increased capacitance after activation), confirming the excellent stability of the electrode and highly reversible NiS/NiSOH redox reaction. Furthermore, as revealed by TEM, the structure of α-NiS/CRs hybrid perfectly preserves after 2000 cycles (Fig. 4c and 4d), certifying that the unique structure can effectively prevent the exfoliation and alleviate the aggregation of the active NPs, thus leading to the excellent cycling stability.

Discussion

We proposed a simple strategy to incorporate α-NiS nanocrystals into carbon nanorods (α-NiS/CRs) by in-situ sulfidation of a Ni-carbon nanorods composite (Ni/CRs) prepared by carbonization of nickel dimethyglyoximate. The nanopore confinement by the carbon matrix is essential for the formation of α-NiS and preventing its transition to β-phase. The hybrid "supercapacitor-battery electrode" materials based on α-NiS/CRs demonstrate high specific capacitance and excellent cycling stability. The outstanding performance can be attributed to 1) the high electrochemical activities and good conductivity of α-NiS; 2) conductive matrix provided by carbon nanorods; 3) dispersed and stable confinement of α-NiS NPs; 4) synergistic use of capacitor and battery components rather than a merely additive composite. This study not only suggests a general approach for phase-controlled synthesis of transition metal sulfides but also opens the door to the rational design and fabrication of novel nickel-based/
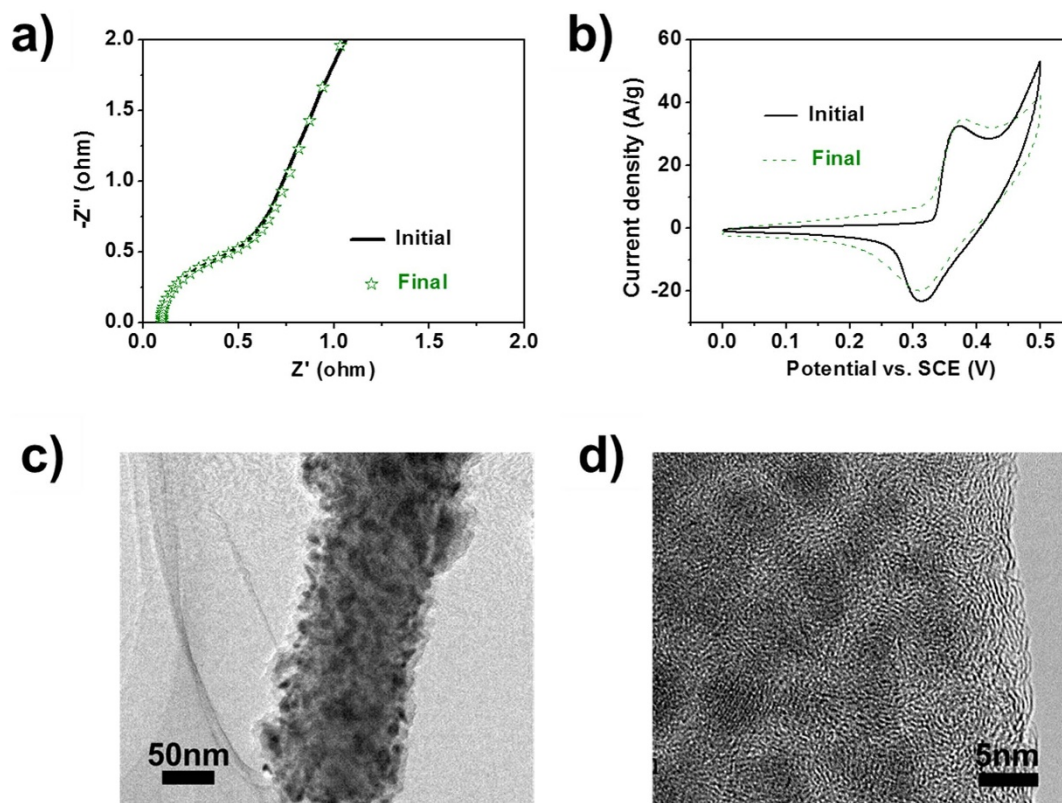

Figure 4 | Electrochemical evolution of the α-NiS/CRs hybrid electrode before and after 2000 charge/discharge cycles. (a) EIS spectra, and (b) cyclic voltammogram curves of α-NiS/CRs composite before and after 2000 charge/discharge cycles. (c) TEM and (d) HRTEM of α-NiS/CRs composite after 2000 charge/discharge cycles.

carbon hybrid supercapacitor-battery electrode materials with enhanced properties.

Methods

Dimethylglyoximate, Nickel chloride ($NiCl_2$), thiourea and glycerol were purchased and used without further purification. All aqueous solutions were freshly prepared with ultra pure water (18 MΩ).

Synthesis of Ni/CRs. As similar to the previous report[39], typically, 0.278 g dimethylglyoxime was dispersed in 24 mL ethanol and the PH value was adjusted to 13.0 by dropping 0.5 mol/L NaOH in ethanol. 0.284 g $NiCl_2$ was dispersed in 800 mL distilled water. Dimethylglyoxime was added into $NiCl_2$ under ultrasonication. After dried, the cotton-like precipitate at 80°C overnight, the sample was carbonized in a tube furnace under argon at 350°C for 1 h.

Synthesis of α-NiS/CRs. α-NiS/CRs was prepared by a facile solvothermal synthesis method,5.0 mg Ni/CRs was dispersed in 50 mL glycerin containing 2.0 mmol thiourea. The solution was refluxed at 280°C for 1 h to ensure the synthesis of α-NiS/CRs. The product was collected by filtration, washed several times with deionized water and then dried at 80°C overnight.

Synthesis of β-NiS/CRs. For comparison, the Ni/CRs composite was immersed into 3.0 M aqueous HCl solution overnight to leave the free-standing MCRs. The nickel NPs were synthesis according to the literature[40]. The synthetic process of β-NiS/CRs composite was same as the α-NiS/CRs except the Ni NPs and MCRs were added separately as the mass ratio of Ni/CRs.

Microscopic Characterization. The crystallographic information of the samples were characterized by X-ray diffraction (XRD) on a Rigaku powder X-ray diffractometer with Cu Kα radiation (λ=1.5418 Å). Morphologies of the samples were investigated on a Hitachi S-4800 field-emission scanning electron microscope (FESEM) at acceleration voltage of 5.0 kV. The morphologies and structures of the samples were further investigated by transmission electron microscopy (TEM) and high-resolution transmission electron microscopy (HRTEM), operated on a JEOL JEM-2100 with acceleration voltage of 200 kV. The nitrogen adsorption-desorption isotherm was conducted using Brunauer-Emmett-Teller (BET) theory by a Mircomeritics ASAP 2020 surface area and porosity analyzer. The pore size distributions were evaluated using Barrett-Joyner-Halenda (BJH) model. The thermogravimetric analysis (TGA) was conducted by Shimadzu-60 thermo-analyzer under air flow at 10°C min-1 from 50°C to 750°C.

Electrochemical Performance measurements. The electrochemical performance was carried out in a CHI660C electrochemical workstation (Chenghua, Shanghai) with 2 M KOH aqueous as the electrolyte at room temperature. A Pt plate and standard calomel electrode (SCE) were used as counter and reference electrode, respectively. The electrochemical impedance spectroscopy (EIS) was performed using an amplitude of 5 mV and frequency range from 500 kHz to 5 mHz. The specific capacitance (C) was calculated according to equation (4):

$$C = \frac{I\Delta t}{m\Delta V} \qquad (4)$$

Where I (mA) the discharge current, and m(g), ΔV (V), Δt (s), the designated mass of active materials, potential drop during discharge, discharge time, respectively.

1. Yuan, C., Wu, H. B., Xie, Y. & Lou, X. W. D. Mixed Transition-Metal Oxides: Design, Synthesis, and Energy-Related Applications. *Angew. Chem. Int. Ed.* **53**, 1488–1504 (2014).
2. Lai, C.-H., Lu, M.-Y. & Chen, L.-J. Metal sulfide nanostructures: synthesis, properties and applications in energy conversion and storage. *J. Mater. Chem.* **22**, 19–30 (2012).
3. Du, J. M. & Kang, D. J. A shape-controlled method to functionalize multiwalled carbon nanotubes with Ni3S2. *Inorg. Chem.* **46**, 10307–10311 (2007).
4. Jiang, X. et al. Synthesis of Novel Nickel Sulfide Layer-Rolled Structures. *Adv. Mater.* **13**, 1278–1281 (2001).
5. Ghezelbash, A., Sigman, M. B. & Korgel, B. A. Solventless synthesis of nickel sulfide nanorods and triangular nanoprisms. *Nano Lett.* **4**, 537–542 (2004).
6. Aso, K., Kitaura, H., Hayashi, A. & Tatsumisago, M. Synthesis of nanosized nickel sulfide in high-boiling solvent for all-solid-state lithium secondary batteries. *J. Mater. Chem.* **21**, 2987–2990 (2011).
7. Kullerud, G. & Yund, R. A. The Ni-S system and related minerals. *J. Petrol.* **3**, 126–175 (1962).
8. Wei, C., Lu, Q., Sun, J. & Gao, F. Evolution of nickel sulfide hollow spheres through topotactic transformation. *Nanoscale* **5**, 12224–12230 (2013).
9. Sun, Y. & Xia, Y. Shape-controlled synthesis of gold and silver nanoparticles. *Science* **298**, 2176–2179 (2002).
10. Puntes, V. F., Zanchet, D., Erdonmez, C. K. & Alivisatos, A. P. Synthesis of hcp-Co nanodisks. *J. Am. Chem. Soc.* **124**, 12874–12880 (2002).
11. Peng, X. et al. Shape control of CdSe nanocrystals. *Nature* **404**, 59–61 (2000).
12. Jiao, F. & Bruce, P. G. Mesoporous Crystalline β-MnO2—a Reversible Positive Electrode for Rechargeable Lithium Batteries. *Adv. Mater.* **19**, 657–660 (2007).
13. Jang, B. et al. Direct synthesis of self-assembled ferrite/carbon hybrid nanosheets for high performance lithium-ion battery anodes. *J. Am. Chem. Soc.* **134**, 15010–15015 (2012).
14. Man, R. W., Brown, A. R. & Wolf, M. O. Mechanism of Formation of Palladium Nanoparticles: Lewis Base Assisted, Low-Temperature Preparation of Monodisperse Nanoparticles. *Angew. Chem. Int. Ed.* **51**, 11350–11353 (2012).
15. Jiang, Q. & Ward, M. D. Crystallization under nanoscale confinement. *Chem. Soc. rev.* **43**, 2066–2079 (2014).
16. Diao, Y., Myerson, A. S., Hatton, T. A. & Trout, B. L. Surface design for controlled crystallization: The role of surface chemistry and nanoscale pores in heterogeneous nucleation. *Langmuir* **27**, 5324–5334 (2011).
17. Duran, H., Steinhart, M., Butt, H.-J. r. & Floudas, G. From heterogeneous to homogeneous nucleation of isotactic poly (propylene) confined to nanoporous alumina. *Nano Lett.* **11**, 1671–1675 (2011).
18. Napolitano, S. & Wübbenhorst, M. The lifetime of the deviations from bulk behaviour in polymers confined at the nanoscale. *Nat. Commun.* **2**, 260 (2011).
19. Hu, Y., Chen, J.-F., Zhang, H.-T., Li, T.-W. & Xue, X. Using silicon dioxide nanosphere gaps to confine growth of single-crystal nickel sulfide nanowires in polyacrylamide gel. *Scr. Mater.* **55**, 131–134 (2006).
20. Hou, L. et al. Electrochemically induced transformation of NiS nanoparticles into Ni (OH)2 in KOH aqueous solution toward electrochemical capacitors. *Electrochim. Acta* **56**, 7454–7459 (2011).
21. Yang, J., Duan, X., Qin, Q. & Zheng, W. Solvothermal synthesis of hierarchical flower-like β-NiS with excellent electrochemical performance for supercapacitors. *J. Mat. Chem. A* **1**, 7880–7884 (2013).
22. Gao, B., Yuan, C., Su, L., Chen, S. & Zhang, X. High dispersion and electrochemical capacitive performance of NiO on benzenesulfonic functionalized carbon nanotubes. *Electrochim. Acta* **54**, 3561–3567 (2009).
23. Tao, D., Richardson, P., Luttrell, G. & Yoon, R.-H. Electrochemical studies of pyrite oxidation and reduction using freshly-fractured electrodes and rotating ring-disc electrodes. *Electrochim. Acta* **48**, 3615–3623 (2003).
24. Zhu, Z. et al. Ultrasmall Sn nanoparticles embedded in nitrogen-doped porous carbon as high-performance anode for lithium-ion batteries. *Nano Lett.* **14**, 153–157 (2013).
25. Zhang, H. et al. Synthesis of Bacteria Promoted Reduced Graphene Oxide-Nickel Sulfide Networks for Advanced Supercapacitors. *ACS Appl. Mat. Interfaces* **5**, 7335–7340 (2013).
26. Jayaprakash, N., Shen, J., Moganty, S. S., Corona, A. & Archer, L. A. Porous Hollow Carbon@ Sulfur Composites for High-Power Lithium-Sulfur Batteries. *Angew. Chem. Int. Ed.* **123**, 6026–6030 (2011).
27. Su, L., Zhou, Z. & Shen, P. Ni/C hierarchical nanostructures with Ni nanoparticles highly dispersed in N-containing carbon nanosheets: origin of Li storage capacity. *J. Phys. Chem. C* **116**, 23974–23980 (2012).
28. Ma, C. et al. The electrochemical performance of pitch coke anodes containing hollow carbon nanostructures and nickel nanoparticles for high-power lithium ion batteries. *Electrochim. Acta* **112**, 394–402 (2013).
29. Zultanski, S. L. & Fu, G. C. Nickel-catalyzed carbon-carbon bond-forming reactions of unactivated tertiary alkyl halides: Suzuki arylations. *J. Am. Chem. Soc.* **135**, 624–627 (2013).
30. Garcia, A. C., Lima, F. H., Ticianelli, E. A. & Chatenet, M. Carbon-supported nickel-doped manganese oxides as electrocatalysts for the oxygen reduction reaction in the presence of sodium borohydride. *J. Power Sources* **222**, 305–312 (2013).
31. Tang, W. et al. An aqueous rechargeable lithium battery of excellent rate capability based on a nanocomposite of MoO3 coated with PPy and LiMn2O4. *Energy Environ. Sci.* **5**, 6909–6913 (2012).
32. Liu, Y. et al. Polypyrrole-coated α-MoO3 nanobelts with good electrochemical performance as anode materials for aqueous supercapacitors. *J. Mater. Chem. A* **1**, 13582–13587 (2013).
33. Zhu, T., Wang, Z., Ding, S., Chen, J. S. & Lou, X. W. D. Hierarchical nickel sulfide hollow spheres for high performance supercapacitors. *RSC Adv.* **1**, 397–400 (2011).
34. Zhi, M., Xiang, C., Li, J., Li, M. & Wu, N. Nanostructured carbon–metal oxide composite electrodes for supercapacitors: a review. *Nanoscale* **5**, 72–88 (2013).
35. Vlad, A. et al. Hybrid supercapacitor-battery materials for fast electrochemical charge storage. *Sci. rep.* **4**, 4315 (2014).
36. Augustyn, V. et al. High-rate electrochemical energy storage through Li+ intercalation pseudocapacitance. *Nat. Mater.* **12**, 518–522 (2013).
37. Zhang, Y. et al. Selective synthesis of hierarchical mesoporous spinel NiCo 2 O 4 for high-performance supercapacitors. *Nanoscale* **6**, 4303–4308 (2014).
38. Tsao, H. N. et al. Influence of the interfacial charge-transfer resistance at the counter electrode in dye-sensitized solar cells employing cobalt redox shuttles. *Energy Environ. Sci.* **4**, 4921–4924 (2011).
39. Bo, X., Zhu, L., Wang, G. & Guo, L. Template-free synthesis of rectangular mesoporous carbon nanorods and their application as a support for Pt electrocatalysts. *J. Mater. Chem.* **22**, 5758–5763 (2012).

40. Chen, D.-H. & Wu, S.-H. Synthesis of nickel nanoparticles in water-in-oil microemulsions. *Chem. Mater.* **12**, 1354–1360 (2000).

Acknowledgments

Author contributions

S.C. and D.X. conceived the idea. S.C. carried out materials fabrication. S.C., M.M., Y.J. and Z.Y. performed materials characterizations. S.C., D.X., C.P. and H.W. drafted the manuscript. All authors analyzed and discussed the experimental results.

Additional information